Left Ventricular Wall Motion Estimation by Active Polynomials for Acute Myocardial Infarction Detection

SERKAN KIRANYAZ[1], (Senior Member, IEEE), AYSEN DEGERLI[2], TAHIR HAMID[3],
RASHID MAZHAR[3], RAYYAN EL FADIL AHMED[1], RAYAAN ABOUHASERA[1],
MORTEZA ZABIHI[1], (Member, IEEE), JUNAID MALIK[2],
RIDHA HAMILA[1], (Senior Member, IEEE), AND MONCEF GABBOUJ[2], (Fellow, IEEE)

[1]Department of Electrical Engineering, Qatar University, Doha, Qatar
[2]Faculty of Information Technology and Communication Sciences, Tampere University, 33720 Tampere, Finland
[3]Heart Hospital, HMC, Doha, Qatar

Corresponding author: Serkan Kiranyaz (mkiranyaz@qu.edu.qa)

ABSTRACT Echocardiogram (echo) is the earliest and the primary tool for identifying regional wall motion abnormalities (RWMA) in order to diagnose myocardial infarction (MI) or commonly known as heart attack. This paper proposes a novel approach, *Active Polynomials*, which can accurately and robustly estimate the global motion of the Left Ventricular (LV) wall from any echo in a robust and accurate way. The proposed algorithm quantifies the true wall motion occurring in LV wall segments so as to assist cardiologists diagnose early signs of an acute MI. It further enables medical experts to gain an enhanced visualization capability of echo images through color-coded segments along with their "maximum motion displacement" plots helping them to better assess wall motion and LV Ejection-Fraction (LVEF). The outputs of the method can further help echo-technicians to assess and improve the quality of the echocardiogram recording. A major contribution of this study is the first public echo database collection composed by physicians at the Hamad Medical Corporation Hospital in Qatar. The so-called HMC-QU database will serve as the benchmark for the forthcoming relevant studies. The results over HMC-QU dataset show that the proposed approach can achieve 87.94% accuracy, 92.86% sensitivity and 87.64% precision in MI detection even though the echo quality is quite poor and the temporal resolution is low.

INDEX TERMS Echocardiogram, left ventricular wall motion estimation, myocardial infarction.

I. INTRODUCTION

Early detection of an acute myocardial infarction (MI) [1], [2] or in general a coronary artery disease (CAD) requires an accurate estimation of the regional and global motion of the left ventricle (LV) of the heart. Early and fundamental signs of a CAD are believed to show in LV wall motion as abnormalities in one or several segments of the LV wall, where a segment may move "abnormally" or "non-uniformly". This abnormality can be defined as a "weak motion", known as *hypokinesia*, "no motion", known as *akinesia* or "out of sync", known as *dyskinesia*. The primary tool to detect, identify and quantify such regional wall motion abnormalities (RWMA) is the patient's echocardiogram (echo), which

is notoriously difficult, and subjective and, therefore, highly operator dependent. Although RWMA is the first abnormality to set in with the onset of myocardial ischemia, preceding metabolic and electrocardiographic abnormalities, it is currently only used as a secondary diagnostic tool in patients with non-diagnostic ECG or when diagnosis is not evidenced (or shown/proven) by "standard" means, despite the fact that echo and particularly myocardial strain imaging provide an early diagnosis of an acute MI when RWMA is present. The reasons for not using echo as a first line diagnostic tool, for suspected MI patients, are largely interpretational. Echocardiographic interpretation, such as ultrasound scan, is highly operator-dependent as it depends upon the visual estimation of the left ventricle (LV) muscle-wall motion, its radial displacement and deformations. As a result, the final diagnosis suffers severely from the high inter-observer and

The associate editor coordinating the review of this manuscript and approving it for publication was Kin Fong Lei.

IEEE *Access*

S. Kiranyaz *et al.*: Left Ventricular Wall Motion Estimation by Active Polynomials for Acute Myocardial Infarction Detection

intra-observer variability, making it prone to human errors and misjudgments.

To address these challenges, there is a need for an automated, robust and accurate tool that can assist cardiologists and echo-technicians understand and interpret echo more accurately, which may lead to saving lives. Despite the need, there are only few studies in the literature which proposed an automatic method for the LV wall motion estimation and abnormality detection from echo [3]. This is not surprising because first of all, there is no publicly available benchmark echo database with ground-truth labels. Second, capturing the global motion of an arbitrary shaped LV segment is difficult especially when the quality and/or spatial/temporal resolution of the echo is low. Finally, "motion estimation" in a video is known to be an *ill-posed* problem [3]–[5] even for natural videos with distinct objects/textures. This is true both for dense (pixel-based) or local (few pixels or block-based) motion estimation. Therefore, for a typical echo, which may be too noisy, estimating the true motion of the entire LV wall from such local (group of) pixels will be difficult and in some cases, impossible [6]. A recent study [7] has attempted to address this problem by two Machine Learning approaches. Both approaches have obtained low accuracies varying 57% to 85.4% and specificities varying 47% to 77.6% despite the fact that the echo videos were in relative high quality and pre-processed.

Due to these limitations and drawbacks, echocardiographic strain and strain-rate imaging (deformation imaging), instead, became the main focus of many studies as a non-invasive method for the assessment of myocardial function. LV wall motion and wall deformation (strain) are different assessments. First of all, while the motion can be estimated and assessed by human experts in a subjective way, this is not possible for the strain because it represents the amount (and rate) of deformation of the LV wall such as longitudinal shortening (negative strain) and radial thickening (positive strain) during myocardial contraction. A human eye, no matter how trained and experienced the practitioner can be, cannot sense or measure this from an echo. On the other hand, strain and strain rate (SR) measurements are also derived from the myocardial velocities over the LV wall. The most common technique is called "Speckle Tracking" [6]–[23], which attempts to capture the motion by tracking "speckles" (natural acoustic markers) in the 2D ultrasonic image (echo). Speckles are the brightest patches and they usually are about 20 to 40 pixels. In prior studies, they are assumed to be "stable" from frame to frame. So, under the assumption of an accurate frame-by-frame tracking, the change of a speckle position gives its velocity and thus the LV wall motion is somewhat reflected by the motion of the speckles. They are chosen at the LV segment borders to produce the motion curves from which (negative) strain (i.e., shortening) and SR can be estimated. Therefore, the accuracy of the strain and SR estimation, too, solely depend on the accuracy of the motion estimation (and tracking) of each joint speckle during one or more cardiac cycles. Although the motion estimation of

a local group of pixels is much easier than the estimation of the global motion of the entire LV wall, it still suffers from this *ill-posed* nature of the problem, e.g., due to small sensor movements, medium to very high noise levels, poor temporal and spatial resolution, and other sources of distortions [6]. For example, the minimum frame rate required for a reasonable speckle tracking is 60 fps. A higher frame rate is another challenge since it reduces the spatial resolution resulting in poor tracking. Moreover, robustness is a crucial issue since it is a well-known fact that different speckle tracking algorithms produce different results. In this study, we shall demonstrate that even when robust key-points are used instead of those speckles, robustness still remains the main problem. Eventually, the curves resulting from strain imaging are highly variable and their interpretation for diagnosis is subjective and experience-dependent [11]. Even under ideal conditions, many studies [11], [19]–[23] reported around 80-85% sensitivity rate for the detection of the infarcted segments. For instance, in an earlier study on 30 patients Leitmann *et al.* [19] found that 80.3% of the infarcted segments and 97.8% of normal segments were adequately recognized by speckle tracking based 2D-strain imaging. Even when the Doppler echo is used, the longitudinal Doppler strain data displayed 85% sensitivity and specificity for the detection of infarcted segments [20]. As a result, despite some promising and recently published studies [21]–[23], strain imaging based on speckle tracking is not ready yet for routine assessment of MI viability [11].

In this study, we propose a novel and fully automatic (unsupervised) Computer Vision method, called *Active Polynomials* (APs) that can capture the global motion of the LV wall in a robust and accurate way. Our objective is to *mimic* an expert cardiologist who can analyze the echocardiogram records by visually searching for any RWMA for the early detection of an acute myocardial dysfunction. While the cardiologist can only perform this subjectively, APs can be used to capture and measure the *true* motion of the LV wall; therefore, it can identify and quantify the regional motion abnormalities. In order to accomplish this, APs are formed on the endocardial boundary of the LV wall and chamber. This boundary is the most promising salient feature of an echo where the maximum contrast usually occurs. In order to capture this boundary, we use the Active Contour (or snake) [24] with an artificial constraint embedded on the LV wall with the Ridge Polynomials (RPs). RPs will ensure a *converging* snake initiated in the LV chamber; however, due to the high noise level, the snake may still partially fail to converge over the endocardial boundary of the LV wall. This is why we shall then fit a 4th order polynomial over the snake in order to obtain the APs that can cover the boundary of the entire LV wall in a smooth and continuous manner. Once this is repeated for all frames in the echo, then the global motion of the segments on the LV wall can be modelled by "motion activity" curves and their maximum displacement can be measured. While the APs can be used as an automatic tool to detect and identify objectively a possible segment motion

S. Kiranyaz *et al.*: Left Ventricular Wall Motion Estimation by Active Polynomials for Acute Myocardial Infarction Detection

IEEE *Access*

abnormality (and hence to identify the infarcted segments causing a possible MI), it can also be used as an enhanced visualization platform over the raw echo to assist cardiologists or echo operators for a more accurate diagnosis and echo quality assessment. Finally, the proposed method is tested extensively over the first benchmark echo dataset, HMC-QU, solely created for this purpose by the physicians in Hamad Medical Corp. (HMC) Hospital and researchers in Qatar University (QU). HMC-QU encapsulates 160 echos, 91 of which are from acute MI patients and the rest from normal (non-MI) patients. HMC-QU is the first publicly available dataset and is the largest by far among the non-public ones used in prior works [6]–[23]. The 4-chamber view echos of the MI patients are labelled by a group of physicians in HMC Hospital, and the proposed method is evaluated based on these ground-truth segment labels of each echo.

The rest of the paper is organized as follows. Section II provides preliminary work on MI detection on echo and Active Contours. Section III presents the proposed LV wall motion estimation for MI detection and identification. The benchmark echo dataset, HMC-QU will first be introduced in Section IV. Then both quantitative and qualitative evaluations of the proposed approach over the HMC-QU dataset will be detailed and the MI detection performance will be analyzed together with a computational complexity analysis. Finally, Section V concludes the paper and suggests topics for future research.

II. PRELIMINARIES

A. MI DETECTION BY LOCAL MOTION ESTIMATION

MI is a major cause of death worldwide and gaining momentum especially during the last decade. In pathology, MI can be defined as myocardial cell death due to prolonged ischemia. When a coronary artery is blocked, the CAD shows the first signs of perfusion abnormalities due to the lack of oxygenated blood flow to the LV tissue within minutes from the occlusion of the coronary artery, leading to severe ischemia, which produces regional wall motion abnormalities (RWMAs). These RWMAs can be visualized by echo. This is the onset of a MI that can be even before the patient feels a chest pain or angina. That is why echo is an essential tool to detect the onset of myocardial ischemia and to identify the arteries with blockage.

In an echo, there are different standardized LV segmentation models, such as 16-segment, 17-segment, and 18-segment models. The American Heart Association Writing Group on Myocardial Segmentation and Registration for Cardiac Imaging recommendation is to use the 17-segment model [18] shown in Figure 1. In this study, the proposed technique has been developed and extensively tested on the 4-chamber view. As illustrated in Figure 2, the LV has 7 segments where 6 of them except the *apical cap* (segment-4) exhibit a uniform motion activity. Prior studies that attempt to compute the longitudinal strain by speckle-tracking echocardiography fix a speckle at each segment boundary and attempt to track it during one or few cardiac cycles. Due to the
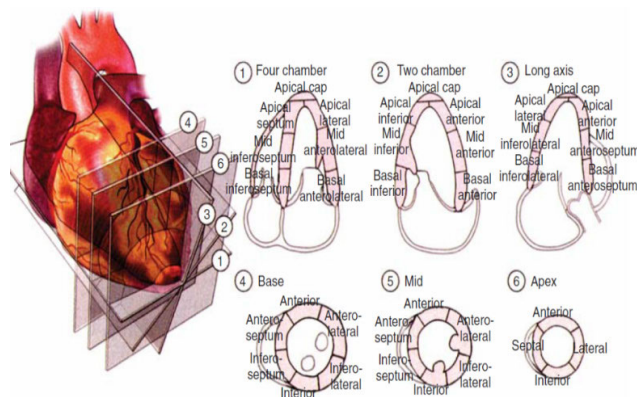

FIGURE 1. The American Heart Association Writing Group on Myocardial Segmentation and Registration for Cardiac Imaging recommendation for the 17-segment model [18].
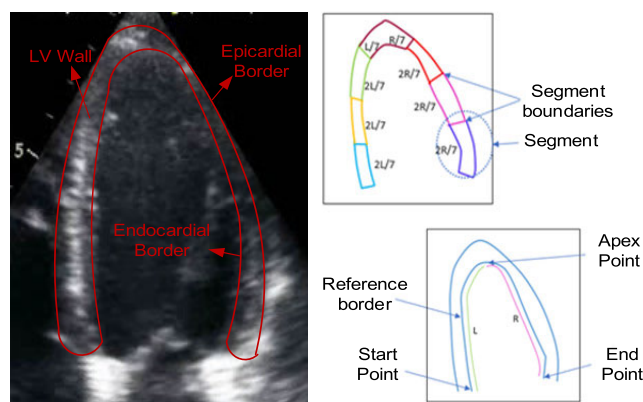

FIGURE 2. The LV wall and its borders (left) in the 4-chamber view. According to the American Heart Association Writing Group on Myocardial Segmentation and Registration for Cardiac Imaging recommendation [18] the segmentation of the LV wall and the start-end points (right).

aforementioned limitations and drawbacks, even in ideal cases (i.e., low noise, high frame rate, and full contrast), the speckle tracking methods can achieve around 80-85% sensitivity and specificity levels.

In this study, we first investigated whether more stable and robust key-points can indeed cure the drawbacks of speckles. So, instead of a motion analysis based solely on a single speckle on each segment boundary along with its local region, we extract a large number of highly robust key-points on the LV wall by using the method called, "Speeded up Robust Feature" (SURF) [25], which belongs to the family of well-known key-point extractors in Computer Vision [25]–[28] including the first and perhaps the most popular one, "Scale Invariant Feature Transform" (SIFT). Juan and Gwun in [25] evaluated the performances of SIFT, PCA-SIFT and SURF methods for scale, rotation, and affine transforms as well as for blur and illumination changes. This study has shown that SIFT performed slightly superior in most experiments but with the slowest speed (highest computational complexity). Some other experiments have shown that SURF was the fastest and the most stable [26]. Obviously, both SIFT and SURF points show a superior robustness over

the naïve speckles with the sole feature of "high brightness" which may change abruptly due to noise, sensor disturbance or other possible factors.

Our aim is to investigate whether a large number of key-points can indeed be used to capture the global motion of the LV wall. Accordingly, we can also find out whether they can be used to compute the strain in a robust and accurate manner. For the former, the results have shown that especially when the noise level is high, even the majority of the robust SURF points may lead to erroneous tracking as shown in Figure 3. While SURF points are coherent and able to capture the global motion for those echos on top of the figure, the zoomed sections of the echos on the bottom clearly show that the majority of the SURF points, despite their robust and stable nature, could not be tracked due to the high level of noise appearing on the next frame. Obviously for the latter aim, tracking of SURF points on the boundaries of the segments may fail too and this will result in erroneous strain computations, which in turn yield misdiagnosis of the heart status. This shows that such "bottom-up" approaches to capture the true motion of the LV wall using the local key-points may neither be robust nor reliable for MI detection. This clearly indicates that the global motion should instead be captured in a "top-down" fashion. The two possible solutions for this approach are the (accurate) segmentation of the LV wall or extraction of the entire endocardial boundary at each frame of the echo. For the latter approach, in an earlier study [29], the anchor points over the LV wall boundaries (both endocardium and epicardium) are manually located and tracked through the rest of the echo. There are few recent attempts for the former using recent Deep Learning paradigms [30]–[33]; however, they cannot still guarantee an accurate segmentation especially when the echo quality is poor. Another interesting attempt was in [34] where a non-rigid image registration method on two-dimensional echocardiographic images was proposed for computing the left ventricle (LV) myocardial motion field over a cardiac cycle. The results were evaluated only over 24 subjects (10 healthy and 14 with pathology).

In this study, we shall focus on the latter, the extraction of the endocardial boundary, which can indeed be performed with a high accuracy using the proposed approach. The starting point for this is the Active Contours [24], which will be reviewed next.

B. ACTIVE CONTOURS

An active contour (or snake) is an elastic 2D spline whose contour is guided by internal (smoothness and curvature) and external (image gradients and edges) constraints. The problem is transferred to the minimization of a joint (total) energy, E_T, that can be expressed as follows:

$$E_T = E_I + \gamma E_X = \int_s (E_I(v(s)) + \gamma E_X(v(s))) \, ds. \quad (1)$$

where E_I is internal and E_X is external energy terms that define the respective constraints, γ is the regularization coefficient. In this study, we used a more recent and improved
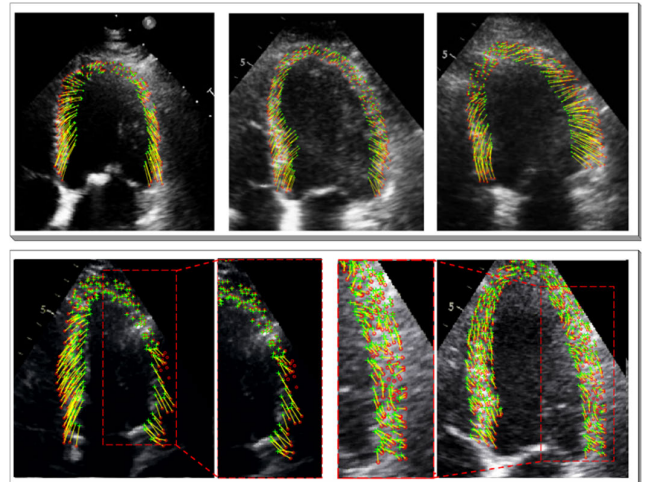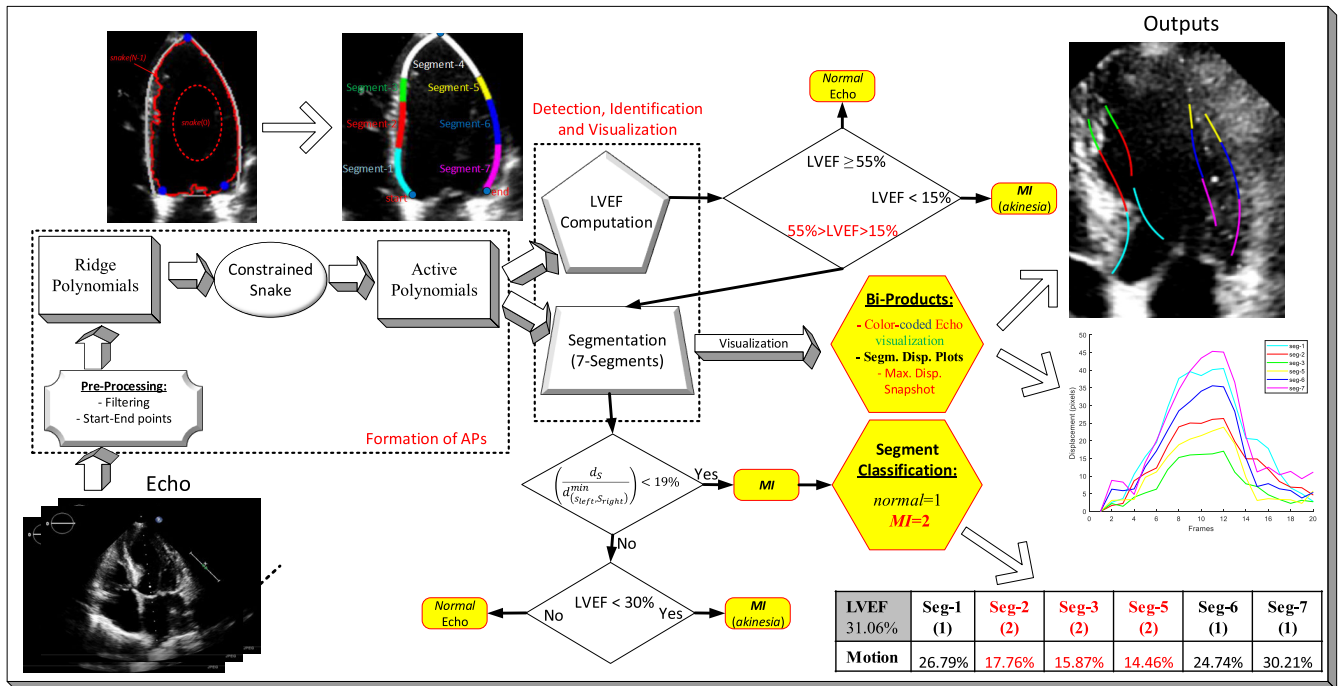

FIGURE 3. Between the consecutive two echo frames, an accurate (top) vs. erroneous (bottom) tracking of the SURF points on the LV wall due to high noise.
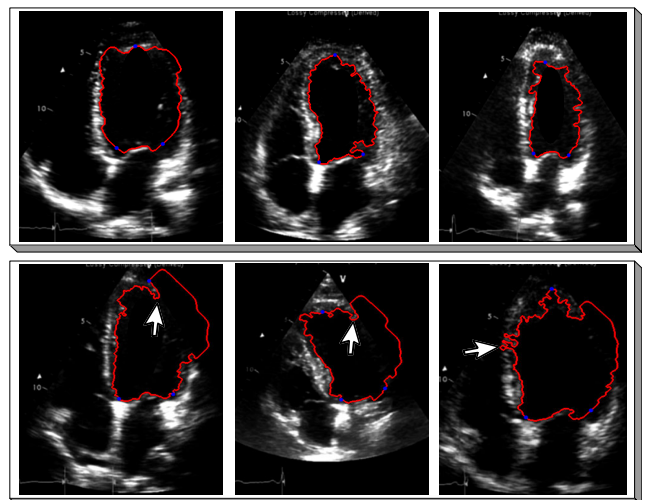
FIGURE 4. Snake method for endocardial LV boundary extraction on 6 echo frames. Reasonable (top) vs. erroneous (bottom) results.

version of snake [34] the details of which are covered in Supplementary (A).

Snake method has been directly used for LV segmentation in a recent study [35]; however, it has only been tested on the frames of a single echo. Although the result was satisfactory, obviously such a limited evaluation is not sufficient. In three studies [37]–[39] a variant of the snake algorithm, the so-called B-spline snake method has been used to compute the left ventricular volume and ejection fraction estimation. Especially when the quality of echo degrades, e.g., excessive noise and/or low or no contrast on the LV wall, the snake may fail to converge to the true boundary of the LV wall. Typical examples can be seen in Figure 4 (bottom) where the snake not only failed to converge to the true boundary due to lack of contrast, it also presents severe noise sensitivity on the boundaries as shown by the white arrows. This basically demonstrates the fact that the "snake-only" approach cannot exhibit the required robustness and accuracy to capture

S. Kiranyaz *et al.*: Left Ventricular Wall Motion Estimation by Active Polynomials for Acute Myocardial Infarction Detection

IEEE *Access*

FIGURE 5. The overview of the proposed method for MI detection and identification. The three end-points are manually pointed for the first frame of the input echo and the RPs and APs are automatically extracted and then used for MI detection. The yellow shaded blocks generate the outputs on the right-most side.

the LV endocardial boundary along with its global motion. In the next section, we shall detail how the proposed method addresses effectively this drawback by using the proposed approach with Active Polynomials (APs).

III. METHODOLOGY

The proposed method consists of two consecutive phases, as illustrated in Figure 5. The first phase is the LV wall extraction. In the second phase, using the APs formed on the LV wall, 7 segments are extracted for MI detection, identification and for further enhanced visualization capabilities to assist cardiologists perform their diagnosis. In the following sections, we shall detail each phase.
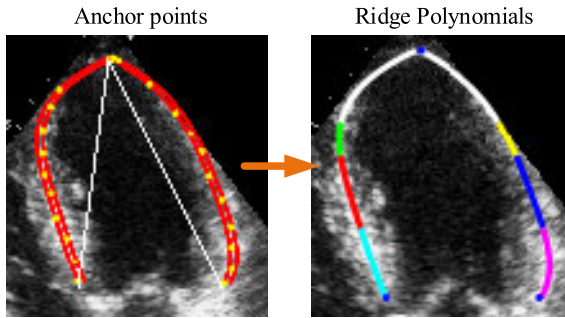
A. LV WALL EXTRACTION

As illustrated in Figure 5, the formation of Active Polynomials (APs) is performed in three stages over each frame of the echo. The first stage is the formation of an artificial wall, Ridge Polynomials (RPs), to prevent the divergence of the snake. The second stage is the formation of the snake within the LV. Finally, the third stage is the composition of the APs over the snake. In the following sub-sections we shall detail each stage.

1) RIDGE POLYNOMIALS

The proposed approach to capture the endocardial boundary is designed to address the two drawbacks of the active contours on echos. The first and the foremost problem is the partial divergence of the snake when the contrast is poor, e.g., see

the three echos in Figure 4 (bottom) where the snake fails to converge to the boundaries of segments 4, 5 and 6. To prevent this, we artificially enhance the contrast by building a white wall on top of the brightest section (i.e., the ridge) of the LV wall. In those problematic echos in the figure, the ridge can even be invisible to the naked eye due to the lack of contrast; however, it still exists with low brightness values while still having the maximum intensity in a local neighborhood. So, the idea is to build a sufficiently thick wall (e.g. 6 pixels) by incrementally increasing the intensity value (e.g. 200 to 255 for 8-bit image representation) on top of the connected series of brightest pixels (i.e. the ridge). To obtain the anchor points on the ridge, we use the *start* and *end* reference points as illustrated in Figure 2 along with the *topmost* point of the *apical cap*. For the first frame of the echo, these three points are manually given. For the 2nd frame onwards until the last frame of the echo, their positions are automatically tracked by the Kanade-Lucas-Tomasi algorithm, which tracks the selected points from the previous to the current frame (forward tracking) and, then to the previous frame again (backward tracking) to compute a bidirectional error. The error is defined as the distance from the original to the final location after the backward tracking. The tracked points are valid when the given threshold (e.g., set to 9 for our case) is satisfied with the final error. In order to determine the other anchor points in between the reference points, as shown in Figure 6 considering that the LV boundary is divided into left and right parts equally from the apex point, two lines are fitted from the top to the start and end points. The ridge

IEEE *Access*

S. Kiranyaz *et al.*: Left Ventricular Wall Motion Estimation by Active Polynomials for Acute Myocardial Infarction Detection

Anchor points   Ridge Polynomials

FIGURE 6. The 14 anchor points (yellow) on LV wall are automatically located at the maximum-intensity points of the LV wall (left). The final ridge polynomial (RP) is then fit over the anchor points (right).

(maximum intensity) points are detected as moving the 14 equally distanced anchor points towards the boundary. New set of anchor points are defined by stretching the anchor points horizontally to obtain a pair of left and right anchor points shown in Figure 6. Finally, over the left and right anchor points, two 4th order ridge polynomials (RPs) are initially fit which will constitute the borders of the search region, i.e., the "Region of Interest" (RoI) inside of which the actual ridge points will be searched. Once the ridge points are detected, the 4th order ridge polynomial is fit to these ridge points using the regularized Least-Square (LS) optimization. The details of fitting an nth order polynomial over $m > n + 1$ points using regularized LS method is given in Supplementary (B). The RPs are then used as the artificial wall (barrier) so that the snake is guaranteed to converge to the LV wall.

2) THE CONSTRAINED SNAKE

As illustrated in Figure 7 (left), the snake is initialized as a mini-form of the RPs within the LV wall which is encapsulated by the actual RPs. After 300 iterations, the snake converges to the true endocardial boundary of the LV wall in Figure 7 (right). In this particular echo, without the artificial wall made by the two RPs, the snake would have diverged on the right side of the LV wall due to lack of contrast of the echo shown in this figure. In this echo and on several others where the snake is divergent, the artificial wall solved this problem. However, the second drawback of the snake approach, the high noise sensitivity, is still evident. The snake may fail to converge to the true boundary due to the noisy speckles within the blood chamber. Furthermore, excess noise level usually makes the snake unnecessarily detailed at the boundaries as shown in Figure 4 (white arrows at the bottom). In order to address these drawbacks, the formation of the proposed Active Polynomials (APs) will be detailed in the next subsection.

3) ACTIVE POLYNOMIALS

Although some sections of the snake suffer from occasional "over-fitting" problem possibly due to the excess noise, even such a problematic snake can still serve as the initial "reference" to capture the endocardial boundary with smooth polynomials.

Left RP   Right RP
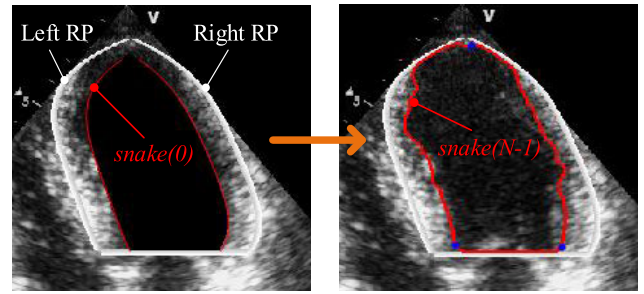
FIGURE 7. The automatic initialization of the snake inside the two RPs (t = 0) and the final snake is converged after N = 300 iterations.
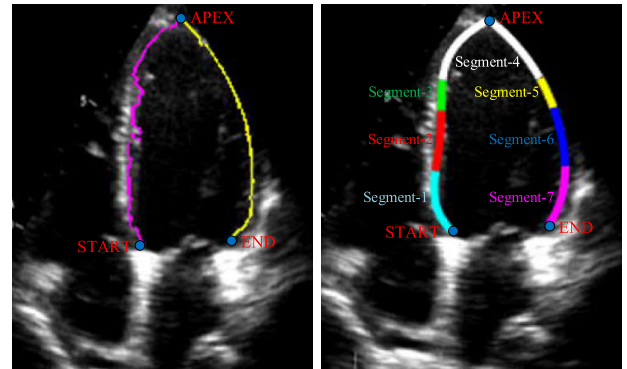
FIGURE 8. Snake points (left) are used to create a pair of APs (right) that are then partitioned into 7 segments of the 4-chamber view.

For this purpose, a pair of 4th order polynomials, for the left and right side of the LV wall are fit to the points of the snake using the regularized LS. For the left one, the 9 equally spaced snake points between the *start* to *apex*, and for the right one, between *apex* and the *end* are used. Since each polynomial will assume a smooth shape of the active contour, we call them Active Polynomials (APs). As shown in Figure 8, the two parts of the snake (purple and yellow) are used to compose a pair of APs and finally, they are used to create 7 segments (segments 1 to 7 counter-clockwise) of the 4-chamber view echo.

B. MI DETECTION, IDENTIFICATION AND VISUALIZATION

This is the second block in Figure 5 which uses the output of the first block, APs, to perform the global motion analysis. APs are divided into 7 segments as shown in Figure 8 (right) and their movement (displacement) is monitored. Once the global motion of each segment is captured by simply evaluating the "rate of displacement", we can mimic a typical cardiologist's diagnosis of a motion anomaly by detecting which segment or segments are showing signs of abnormal (non-uniformity or lack of) motion activity. However, before going into motion analysis, the LV Ejection-Fraction (LVEF) ratio is first computed as follows:

$$LVEF = \frac{EDV - ESV}{EDV} \approx 1 - \frac{A_{min}}{A_{max}} \quad (2)$$

where *EDV* and *ESV* are the end-diastolic and end-systolic volumes, respectively. In a 2D echo, one can estimate them

S. Kiranyaz *et al.*: Left Ventricular Wall Motion Estimation by Active Polynomials for Acute Myocardial Infarction Detection

IEEE *Access*

by computing A_{min} and A_{max}, which are the minimum and maximum area of the LV chamber, respectively. They are proportional to the total number of pixels encapsulated by the snake or by the two APs. The recommendation for *LVEF* to indicate a "reference" (normal) and "severely abnormal" LV activities for both men and women, are LVEF $\geq$ 55% and LVEF $<$ 30%, respectively [40]. Following this recommendation, the proposed motion analysis will no longer be performed when LVEF $\geq$ 55% and the echo can directly be classified as *normal*. However, for the lower limit, we empirically use a more conservative threshold, LVEF $\leq$ 15, which is obviously a sensitive marker of myocardial dysfunction and a clear sign of MI. For this severe case of myocardial dysfunction, the echo with all the segments can directly be classified as MI. Therefore, motion analysis will *only* be performed when 55% > LVEF > 15% and the outcome of the motion analysis will determine whether the echo is normal or MI. In this case, if there is *at least* one myocardial segment with abnormal (*hypokinesia* or *akinesia*) motion activity then MI is detected and the corresponding arteries with blockage can be identified.

When a cardiologist visually evaluates the motion activity of a 4-chamber view echo, the infarcted segments that show a "reduced" motion (or almost no motion at all) compared to other segments are identified either as *hypokinesia* or *akinesia*. The motion assessment is obviously independent from the resolution of the echo. The study over the segments labeled as *abnormal* by the cardiologists in HMC-QU database has indicated that those segments that move less than 20% of the minimum interval to the corresponding segment on the other side of the chamber are diagnosed as MI. Since the minimum interval between corresponding segments is resolution dependent, the ratio of maximum displacement to this minimum interval will therefore allow us to mimic the cardiologist's evaluation in a quantitative way.

Let d_S be the maximum displacement of the segment, S where $S \in \{1, 2, 3, 5, 6, 7\}$. Let $d_{(S_{left}, S_{right})}^{min}$ be the minimum interval during a cardiac cycle of an echo of the corresponding segments, S_{left} and S_{right} where $S_{left} = 1, 2 \, or \, 3$ and $S_{right} = 5, 6 \, or \, 7$, respectively. Since the maximum motion (of a segment), d_S, is proportional to the (maximum) displacement occurred from *end-diastole* to *end-systole*, the proposed method computes d_S as the maximum displacement of each segment and normalizes them by $d_{(S_{left}, S_{right})}^{min}$. Both measurements are one-pixel accurate and the ratio is then compared with an empirical threshold (e.g., 19%) that is selected just below 20%.

Figure 9 illustrates a sample echo from a MI patient where cardiologists labeled segment 3 as *akinetic*, and the rest as *normal*. The two APs extracted for the frames corresponding to *end-diastole* and *end-systole* are shown in the figure. Knowing the *end-diastole* as the first frame, one can easily find the frame of the *end-systole* by simply searching for the maximum overall segment displacement. However, in this study instead of considering the segments in the *end-systole* frame, we search for the maximum displacement of each
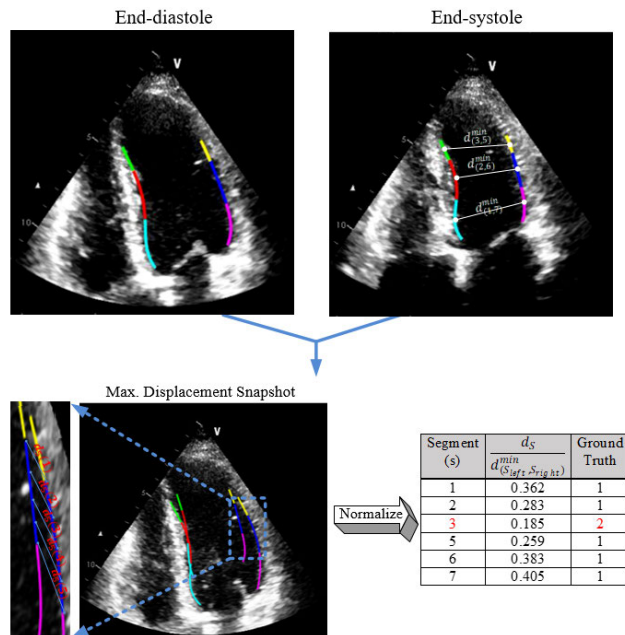
FIGURE 9. Computation of the normalized maximum displacement of the 6 segments of the 4-chamber view echo with the ground-truth labels (normal = 1, infarcted = 2). The normalized motion ratio is computed for each segment by measuring the maximum displacement of the uniformly sampled $n_S = 5$ points on the segment.
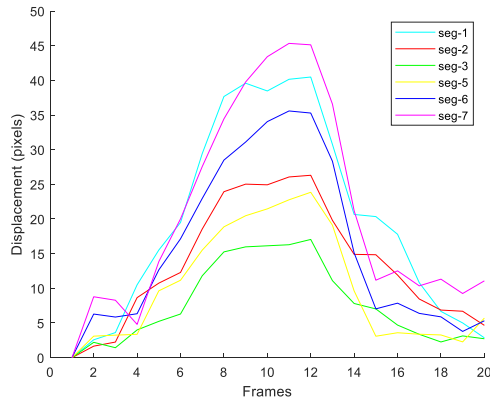
individual segment, which may not necessarily come from the *end-systole* frame. Experiments show that most of the segment-wise maximum displacement indeed occurs at the *end-systole* frame; however, occasionally it may also occur at the frames within a close vicinity (e.g., $\pm$1-2 frames). It is straightforward to notice the "reduced" motion from the gap between $\left(\frac{d_S}{d_{(S_{left}, S_{right})}^{min}}\right)$, ratios of segment 2 and the rest where the latter group has ratios above 19%. Therefore, the results are in full agreement with the ground-truth labels made by the cardiologists.

In order to compute the maximum displacement of a segment, at first, uniformly sampled n_S points are taken over the segment and then the segment displacement can be approximated by averaging the point-wise distances, as expressed below for the 6th segment ($S = 6$) shown in the figure (e.g., for $n_S = 5$).

$$d_S = \frac{1}{n_S} \sum_{i=1}^{n_S} d_S(i) \tag{3}$$

where $d_S(i)$ is the ith point's maximum displacement of the segment $S = 2$ as shown in the figure. There are several options to compute individual point-wise distances, $d_S(i)$. When they visually assess echo, cardiologists consider the motion in both x and y directions. Therefore, we can use L_1, L_2 or L_∞ norms to compute d_S which are expressed as below.

$$d_{L_1} = |x_2 - x_1| + |y_2 - y_1|$$
$$d_{L_2} = \sqrt{(x_2 - x_1)^2 + (y_2 - y_1)^2}$$
$$d_{L_\infty} = max\left(|x_2 - x_1|, |y_2 - y_1|\right) \tag{4}$$

IEEE *Access*

S. Kiranyaz *et al.*: Left Ventricular Wall Motion Estimation by Active Polynomials for Acute Myocardial Infarction Detection

FIGURE 10. Segment displacement plots (normalized motion of each segment vs frame no.) drawn for one cycle (end-systole to end-diastole) for the echo shown in Figure 9.

where (x_1, y_1) and (x_2, y_2) are the x- and y-coordinates of the corresponding i^{th} points on the segment at the *end-diastole* and *end-systole* frames, respectively. A closer look will reveal the fact that $d_{L\infty}$ does not exactly mimic the aforementioned way the cardiologist assess motion since $d_{L\infty}$ only reflects the distance in either x- or y-direction. Between the remaining norms, we use the L_2 norm for maximum displacement calculation since it is the natural distance metric for the human perception. On the other hand, the minimum interval during a cardiac cycle is calculated using L_1 norm in order to fit the ratios of segments in [0,1] more precisely.

An alternative way to assess the segment motion is the segment displacement plots as shown in Figure 10, which show the displacement of each segment during one cardiac cycle. This plot is in fact more informative than the maximum motion ratios given in Figure 9 because the instantaneous and average motion of each segment can also be computed besides their maximum displacements. However, we still perform our motion analysis based on the maximum displacement due to the simple fact that the derivative operator is noise sensitive and the displacement curves will inevitably bear certain level of measurement noise.

Finally, the proposed method presents several enhanced visualization options that will significantly assist medical experts perform their diagnosis. For instance, the color-coded segments formed over the two APs provide a cardiologist with a better motion estimation than the one from the raw (gray-scale) echo since the cardiologist can now see, distinguish and assess each individual segment displacement and (instantaneous) motion in a visually enhanced manner. Another bi-product of the proposed method is the maximum displacement snapshot as shown in Figure 9, which allows cardiologists to visualize the displacement anomaly.

IV. RESULTS
A. HMC-QU BENCHMARK DATASET
HMC-QU benchmark echo dataset has been created by collaboration between Qatar University (QU) and Hamad Medical Corporation (HMC) Hospital in Doha, Qatar. The local

ethics board of (HMC reviewed the study and approved the use of the echo data in February, 2019. HMC-QU contains 160 4-chamber view echo recordings obtained at the HMC hospital between 2018 and 2019. These cases are from over 10000 echos performed in a year including more than 800 cases admitted with acute ST elevation Myocardial infarction. The echos included in our assessment belonging to the 91 MI patients (all first time and acute MI) and the rest are normal. There are 13 women and 76 men in the MI patient group. All MI echos were obtained from patients who were admitted with a diagnosis of acute MI with evidence obtained from ECG, cardiac enzymes and who underwent coronary angiogram/angioplasty to treat the MI. These patients had echos obtained within 24 hours of admission or in some cases before they underwent coronary angioplasty. All "normal" echos were defined, as the echos of the patients not admitted for MI (acute or previous) but acquired for other reasons including health check and investigation of murmurs. All 4-chamber view echos have been labelled segment-wise by cardiologists in HMC hospital. The 6 segments of 4-chamber view of each echo is labelled as: *normal*=1, *hypokinetic*=2 and *akinetic*=3. Echos are acquired by devices from different vendors, such as Phillips Ultrasound machines and GE Vivid (GE-Healthcare-USA) *Ultrasound Machine.* The temporal resolution (frame rate per second) of the echos is 25 fps. The spatial resolution also varies from 422×636 to 768×1024 pixels. The duration of each echo taken for analysis is one cardiac cycle.

B. EXPERIMENTAL SETUP AND RESULTS
In this study, each echo is categorized as *normal* or *MI* while each segment in a 4-chamber view echo is categorized as *normal* (1) or *infarcted* (either *hypokinesia* = 2 or *akinesia* = 3). As illustrated in Figure 5 the motion analysis is only performed if 15% < LVEF < 55%. If LVEF ≥ 55%, all segments are assumed to be *normal* (1) and if LVEF ≤ 15% all segments are assumed to be *akinetic*. Otherwise, the motion analysis will determine whether the echo is *normal* or *MI*. If there is at least one infarcted segment with abnormal motion activity, then the echo is assumed to be *MI*; otherwise, *normal*. A segment is assumed to be *infarcted* if its motion ratio is below 19%. The thresholds, 55% and 30% for LVEF are recommended in [40]. Once all echos in the dataset together with their segments are categorized by the proposed algorithm, then the confusion matrices (CM) are formed by evaluating the assigned categories with respect to the ground-truth labels. This enables us to compute the following standard performance metrics for MI detection and infarcted segment identification performances: classification accuracy (*Acc*), sensitivity (*Sen*), specificity (*Spe*), and positive predictivity (*Ppr*). CM elements are the hit/miss counters such as true positive (*TP*), true negative (*TN*), false positive (*FP*), and false negative (*FN*). The following standard performance metrics can now be expressed using them: *accuracy* is the ratio of the number of correctly detected echos (or segments) to the total number of echos (segments); *sensitivity*
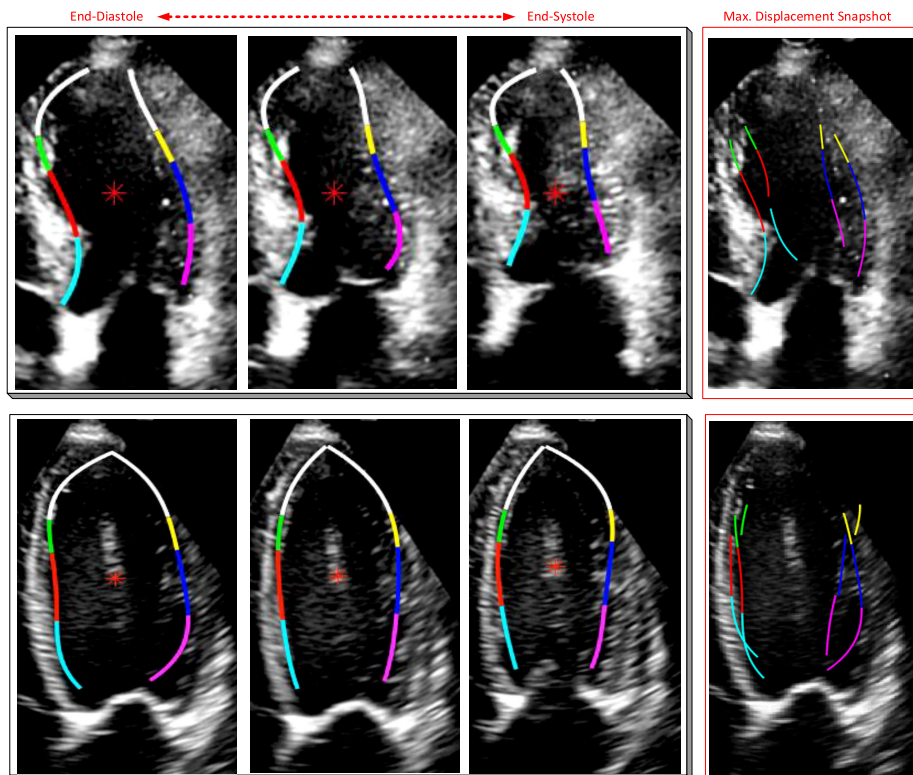
S. Kiranyaz *et al.*: Left Ventricular Wall Motion Estimation by Active Polynomials for Acute Myocardial Infarction Detection

IEEE *Access*

FIGURE 11. End-diastole, middle and end-systole frames of a normal (top) and MI (bottom) echos. Their maximum displacement snapshots are shown on the right.

TABLE 1. The performance of the proposed method (per-segment) on detecting the infarcted segments.

Segment	Sensitivity	Specificity	False alarm	Precision	F1-score	Accuracy
1	0.8929	0.9318	0.0682	0.7353	0.8065	0.9250
2	0.7547	0.8785	0.1215	0.7547	0.7547	0.8375
3	0.8472	0.8750	0.1250	0.8472	0.8472	0.8625
5	0.8519	0.9263	0.0737	0.8679	0.8598	0.8993
6	0.6774	0.9194	0.0806	0.6774	0.6774	0.8710
7	0.6842	0.9281	0.0719	0.5652	0.6190	0.8987

TABLE 2. The performance of the proposed method on detecting the infarcted segments.

Sensitivity	Specificity	False alarm	Precision	F1-score	Accuracy
0.8016	0.9124	0.0876	0.7744	0.7878	0.8822

(or *Recall*) is the rate of correctly detected MI echos among all MI echos in the dataset; *specificity* is the *sensitivity* of the normal echos; and, *positive predictivity* (or *Precision*) is the rate of correctly detected MI echos in all the echos detected as MI. Finally, the *false alarm rate* (*FAR*) can be defined as: $FAR = 1 - Spe$.

Figure 11 shows the *end-diastole*, middle and *end-systole* frames of a *normal* and *MI* echos where the 7 segments are color-coded over the two APs along with their maximum displacement snapshots. The relative motion (displacement)

of the segments 1, 2, 3 and 5 makes it straightforward to detect the motion abnormality on the MI echo while apparently all segments of the *normal* echo move in a uniform manner. Despite the fact that the quality is quite poor with a significant noise in the interior (blood) chamber and the temporal resolution is low (25 fps) in both echos, the proposed method successfully captures the global motion of the LV wall.

The MI detection and identification (detection of the segments with abnormal motion activity) performances are presented in Table 1 (per segment), Table 2 (over all segments)

IEEE *Access*

S. Kiranyaz *et al.*: Left Ventricular Wall Motion Estimation by Active Polynomials for Acute Myocardial Infarction Detection

TABLE 3. MI detection performance of the proposed method over the HMC-QU benchmark dataset with 160 echos.

Sensitivity	Specificity	False alarm	Precision	F1-score	Accuracy
0.8901	0.7536	0.2464	0.8265	0.8571	0.8313
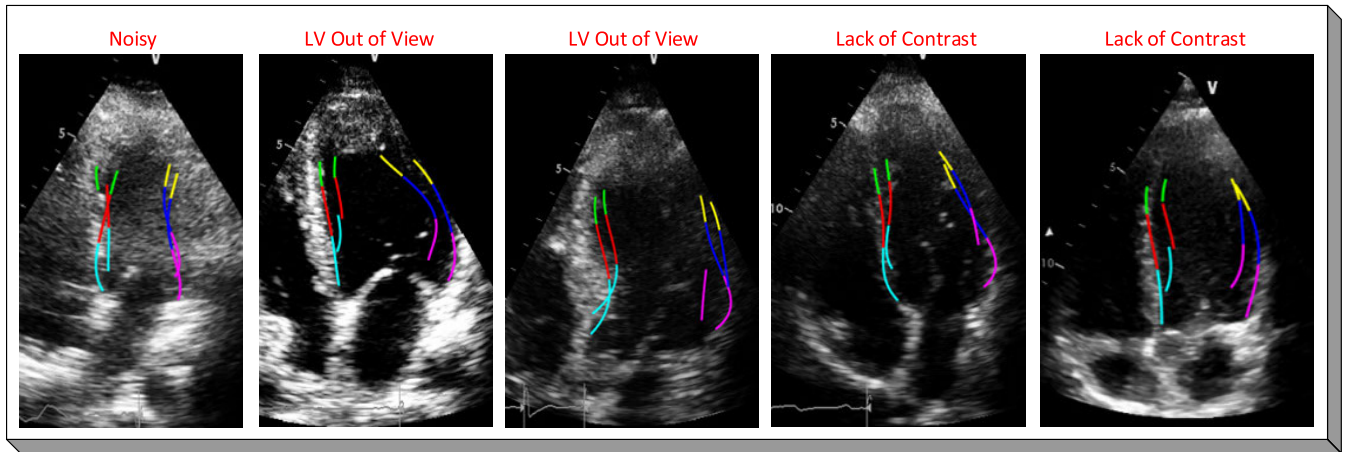
FIGURE 12. A frame from the 5 (out of 19) echos with severe quality problems such as excess noise, LV segments out of view and lack of contrast.
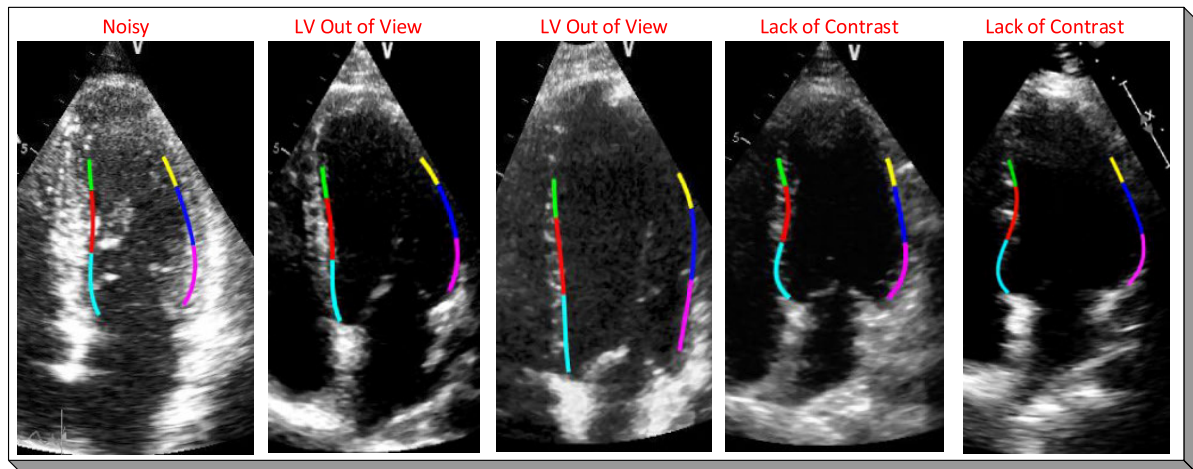
FIGURE 13. Typical low-quality echos in HMC-QU dataset.

TABLE 4. The performance of the proposed method (per-segment) on detecting the infarcted segments over echos with a reasonable quality.

Segment	Sensitivity	Specificity	False alarm	Precision	F1-score	Accuracy
1	0.9259	0.9386	0.0614	0.7813	0.8475	0.9362
2	0.7800	0.8791	0.1209	0.7800	0.7800	0.8440
3	0.8806	0.9189	0.0811	0.9077	0.8939	0.9007
5	0.9000	0.9341	0.0659	0.8824	0.8911	0.9220
6	0.7500	0.9381	0.0619	0.7500	0.7500	0.9007
7	0.7500	0.9360	0.0640	0.6000	0.6667	0.9149

and Table 3 (over all echos), respectively. Several important observations can be made based on these results. First of all, all results are based on the selected motion ratio threshold,

19%. No optimization or fine-tuning was performed on this threshold for maximizing certain criteria. The high accuracies achieved for detecting infarcted segments and echos approve

S. Kiranyaz *et al.*: Left Ventricular Wall Motion Estimation by Active Polynomials for Acute Myocardial Infarction Detection

IEEE *Access*

TABLE 5. The performance of the proposed method on detecting the infarcted segments over echos with a reasonable quality.

Sensitivity	Specificity	False alarm	Precision	F1-score	Accuracy
0.8445	0.9260	0.0740	0.8171	0.8306	0.9031

TABLE 6. MI detection performance of the proposed method over echos with a reasonable quality in the HMC-QU benchmark dataset.

Sensitivity	Specificity	False alarm	Precision	F1-score	Accuracy
0.9286	0.8070	0.1930	0.8764	0.9017	0.8794

the validity of this threshold; however, there is still room for improvement. The most crucial performance criterion is of course *sensitivity* (*Recall*) for infarcted segments and especially MI echos. Especially the latter, *Sen(MI)* > 91%, indicates an elegant performance level considering the low temporal resolution and the poor quality of many echos in the dataset. The secondary objective is to minimize the false alarms (or equivalently to maximize the *specificity*). This is a misdiagnosis case for MI, which can be corrected by the cardiologists when the proposed method causes a false alarm. The *FAR* was rather low (i.e., < 9%) for detecting segment motion abnormality; however, the results in Table 3 show a rather high *FAR*. The main reason is that mis-diagnosing a normal segment as infarcted suffices to misclassify the echo as MI. On the other hand, the fixed threshold used for detection, 19%, may yield such misdiagnosis because the proposed method has a certain sensitivity for capturing the global motion, i.e., in the vicinity of ± 2 pixels and, therefore, a slight variation from the actual displacement may cause such a misclassification even if it is as low as 1-2 pixels, e.g. assume that for a normal segment, $d_{(S_{left}, S_{right})}^{min} = 100\ pixels$ and d_S is measured as 18 pixels with $+2$ pixels bias. Since $\left(d_S / d_{(S_{left}, S_{right})}^{min}\right) = 18\% < 19\%$, this will cause a false alarm.

The main reason for some of the false alarms encountered was the extremely poor image quality of some of the echos in the dataset (19 out of 160), which degrades significantly the actual performance level of the proposed method. Figure 12 shows some sample maximum displacement snapshots of these echos where the echo frames are degraded with excessive noise, lack of contrast or "out-of-view" segments. In such cases, even an expert cardiologists may not perform an accurate diagnosis on these echos. The reason we have included them in the dataset is to accomplish a realistic case and show the main source of misdiagnosis. When those 19 echos with such poor quality are excluded from the evaluation, the actual performance of the proposed method is presented in Table 4, Table 5 and Table 6. However, many of the echos in the database are just slightly better than these 19 echos. For instance, Figure 13 shows 5 sample echos with similar issues, perhaps only slightly lesser. Finally, the poor temporal resolution is also the common drawback among all the echos and as discussed earlier, this, alone, is sufficient

to render out the usage of any method based on Speckle Tracking or local motion estimation. The results presented in the above tables indicate that the proposed approach is quite robust against this drawback and certain level of quality degradations.

C. COMPUTATIONAL COMPLEXITY ANALYSIS
Due to the unoptimized and sequential execution of the proposed method, its computational complexity is the sum of the individual computational complexities of the individual blocks illustrated in Figure 5. Please refer to Supplementary (C) for the computational complexity of each block along with the overall computational times in an unoptimized implementation.

V. CONCLUSION AND FUTURE WORK
In this study, we propose a global method for estimating the true motion of the LV wall by Active Polynomials which are formed at the endocardial boundary of the LV wall for each frame of an echo. Since the proposed method does not depend on local motion estimation and tracking, it is largely immune to the well-known ill-posed behavior and noise sensitivity of the 2D motion estimation. The proposed method is designed to "mimic" an expert cardiologist to capture the global motion in a similar manner so as to assess the regional motion with respect to the motion uniformity. The global extraction of the true motion of the LV wall enables to detect and identify the regional wall motion abnormalities (RWMA) which in turn can diagnose a myocardial infraction (MI) in an objective way. Since echo is the primary tool that can indicate the onset of a Myocardial Ischemia long before the ECG, this will help the detection of a MI at the earliest possible stages -practically as soon as the echo is acquired. Moreover, the proposed method voids the subjectivity and operator dependability of the echo interpretation and assessment since it can quantify the true measures of LV wall motion, (maximum) displacement and LVEF. Besides a standalone diagnostic tool, the proposed method can also offer several assistive bi-products such as enhanced visualization capabilities by color-coded APs over the raw echo, a snapshot of the maximum segment displacements to localize the motion abnormalities, segment displacement plots that can provide a deeper motion analysis and even a quality assessment

tool for the echo acquisition. The last feature is especially important since an echo technician can fine-tune the echo probe manually until the proposed method can successfully compose the APs over the LV wall boundary. Especially, when the diagnosis of the proposed method and the (group of) cardiologist(s) differs, it can also be used as a "verification" tool that can give a second chance to the cardiologists to re-assess the cases or segments with mismatching diagnosis. Finally, when a range is used instead of a fixed threshold for classifying the segments, the proposed method can draw the attention for the *Unsure* cases where the segment motion is not definitive. Cardiologists can handle such difficult cases and make the final decision perhaps by assessing other echo views.

A crucial objective of this study is to achieve an utmost robustness against the high noise level in echos with a poor temporal resolution. Experiments over such echos show that this objective has been well-accomplished. This is particularly important because it is infeasible to analyze such echos with the current state-of-the-art MI detection methods such as "Speckle Tracking" or any other method based on local motion estimation. This has been verified in this study by a case study using the SURF key-points for tracking. Finally, for a proper performance evaluation, the HMC-QU dataset contains ground-truth labels. This is not only the first benchmark dataset that will be publicly available for the research community, it is also the largest collection ever compiled which consists of normal echos and echos of both male and female acute MI patients with different ages. An extensive set of experiments over this benchmark dataset demonstrates that the proposed method achieves an 95.12% sensitivity and 87.64% precision for detecting MI and diagnosing the RWMA. For the latter, specificity is quite high yielding a low false-alarm rate. However, for the MI detection, the proposed method yields a significant false alarm rate; although not as severe as the false negatives, we aim to reduce false alarms with the joint analysis of the other views. Moreover, we aim to improve the speed of the proposed method by parallel computing paradigms and optimized implementation to achieve real-time analysis of the acquired echo. We expect to achieve an even better detection and identification performance with a proper analysis on the motion curves using a Machine Learning approach. These will be the topics of our future work.

SUPPLEMENTARY MATERIAL

A. ACTIVE CONTOURS
In this study, we used a recent variation of snake method proposed in Chan-Vese, [40]. In this variant, the problem defined by [40] is the minimization of an energy-based segmentation. Consider a bounded open subset Ω of $\mathbb{R}^2$, the image $u_0 : \overline{\Omega} \to \mathbb{R}$, the evolving curve C in Ω, as the boundary of an open subset ω of Ω. Then, the *inside*(C) represents the region ω, and *outside*(C) is the region $\Omega\bar{\omega}$. The boundary of the image u_0 is denoted as C_0. Then, the fitting term, F is defined as in Eq.(5) where C the snake curve, and the variables is c_1, c_2 are

the averages of u_0 inside C and outside C, respectively.

$$F_1(C) + F_2(C) = \int_{inside(C)} |u_0(x, y) - c_1|^2 \, dxdy$$
$$+ \int_{outside(C)} |u_0(x, y) - c_2|^2 \, dxdy \quad (5)$$

In this case, the optimal curve is the boundary of the image C_0 which is also the minimizer term in the Eq. (6) as follows:

$$\inf_C \{F_1(C) + F_2(C)\} \approx 0 \approx F_1(C_0) + F_2(C_0) \quad (6)$$

By adding some regularization terms to the minimization equation above, the final energy functional $F(c_1, c_2, C)$ is defined by,

$$F(c_1, c_2, C) = \mu.Length(C) + v.Area(inside(C))$$
$$+ \lambda_1 \int_{inside(C)} |u_0(x, y) - c_1|^2 \, dxdy$$
$$+ \lambda_2 \int_{outside(C)} |u_0(x, y) - c_2|^2 \, dxdy \quad (7)$$

where $\mu \geq 0$, $v \geq 0$ and $\lambda_1, \lambda_2 > 0$ are the fixed parameters. Therefore, the minimization problem proposed by the Chan-Vese method is as follows,

$$\inf_{c_1, c_2, C} F(c_1, c_2, C). \quad (8)$$

The problem can be redefined in a level set form where $C \subset \Omega$ represented by $\phi : \Omega \to \mathbb{R}$ as;

$$\begin{cases} c = \partial\omega = \{(x, y) \in \Omega : \phi(x, y) = 0\} \\ inside(C) = \omega = \{(x, y) \in \Omega : \phi > 0\} \\ outside(C) = \Omega\backslash\bar{\omega} = \{(x, y) \in \Omega : \phi < 0\} \end{cases} \quad (9)$$

The evolution of curve, C in the above level of set functions of Eq.(9) is illustrated in Figure 14 which also reflects the relation between Chan-Vese [34] and Kass *et al.* [24] methods. Using the Heaviside function, H in Eq.(10) and Dirac measure, δ_0 in Eq. (11) the energy function can be rewritten as Eq.(12),

$$H(z) = \begin{cases} 1, & z \geq 0 \\ 0, & z < 0 \end{cases} \quad (10)$$

$$\delta_0(x) = \frac{d}{dz}H(z) \quad (11)$$

$$F(c_1, c_2, \phi) = \mu \int_\Omega \delta(\phi(x, y)) |\nabla\phi(x, y)| \, dxdy$$
$$+ v \int_\Omega H(\phi(x, y))dxdy$$
$$+ \lambda_1 \int_\Omega |u_0(x, y) - c_1|^2 H(\phi(x, y)) \, dxdy$$
$$+ \lambda_2 \int_\Omega |u_0(x, y) - c_2|^2 (1 - H(\phi(x, y)))$$
$$\times dxdy \quad (12)$$

The variables c_1 and c_2 are fixed, and the energy function in Eq.(12) is minimized with respect to ϕ which concludes
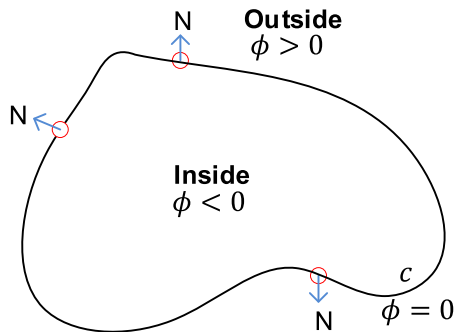
S. Kiranyaz *et al.*: Left Ventricular Wall Motion Estimation by Active Polynomials for Acute Myocardial Infarction Detection

IEEE *Access*

FIGURE 14. The propagation of curve C = {(x, y) : φ(x, y) =} in normal direction.

the Euler-Lagrange equation for ϕ. The descent direction is chosen as an artificial time t where the partial differentiation equation is expressed as follows;

$$\therefore \frac{\partial \phi}{\partial t} = \delta(\phi) \left[\mu div \left(\frac{\nabla \phi}{|\nabla \phi|} \right) - v \right.$$
$$\left. - \lambda_1 (u_0 - c_1)^2 + \lambda_2 (u_0 - c_2)^2 \right]$$
$$= 0 \ in \ (0, \infty) X \Omega,$$
$$\frac{\delta(\phi)}{|\nabla \phi|} \frac{\partial \phi}{\partial \vec{n}} = 0 \ on \ \partial \Omega \qquad (13)$$

where $\vec{n}$ represents the exterior normal to the boundary $\partial \Omega$, and $\frac{\partial \phi}{\partial \vec{n}}$ denotes the normal derivative of ϕ at the boundary. Lastly, Eq.(13) can converge to its solution by gradient descent method.

B. REGULARIZED LEAST-SQUARE FOR n^{th} ORDER POLYNOMIAL FITTING

Assume that we have m points in 2D surface, $p_i = (x_i, y_i)$, $i = 1..m$, and we want to fit n^{th} order polynomial where $m \gg n$. The nth order polynomial, $P(x)$ can be expressed with $n + 1$ coefficients as follows:

$$y = P(x) = \sum_{k=0}^{n} c_k x^k \qquad (14)$$

One can turn this to a LS optimization problem by minimizing the total error,

$$c^{LS} = \min_{c \in R^{n+1}} \|y - P(x)\|^2 = \min_{c \in R^{n+1}} \left(\sum_{i=1}^{m} (y_i - P(x_i))^2 \right) \qquad (15)$$

By defining the matrix, A coefficient vector, x and output vector, b, this problem can be turned to a linear system as,

$$\begin{bmatrix} 1 & x_1 & x_1^2 & x_1^3 & \dots & x_1^n \\ 1 & x_2 & x_2^2 & x_2^3 & \dots & x_2^n \\ 1 & x_3 & x_3^2 & x_3^3 & \dots & x_3^n \\ \dots & \dots & \dots & \dots & \dots & \dots \\ 1 & x_m & x_m^2 & x_m^3 & \dots & x_m^n \end{bmatrix} \begin{bmatrix} c_0 \\ c_1 \\ c_2 \\ \dots \\ c_n \end{bmatrix} = \begin{bmatrix} y_1 \\ y_2 \\ y_3 \\ \dots \\ y_m \end{bmatrix} \qquad (16)$$

or equivalently in a linear system equation,

$$A_{m \times (n+1)} c_{n+1} = b_m \qquad (17)$$

where A is the $mx(n+1)$ matrix with the nth power of the x coordinates of the 2D points are the elements of the $(n + 1)$-dimensional column vector, c, of the polynomial coefficients, (c_u) and b is the m-dimensional column vector of y coordinates of the 2D points. For $m > n + 1$, this is clearly an over-determined linear system, which means that there are more constraints (linear equations) than unknowns (parameters). In such systems there is no (exact) solution, one may only get a *unique* least-square (LS) solution as defined in Eq. (15) or equivalently, the LS solution of this equation, c^{LS}, can be expressed as follows:

$$c^{LS} = \min_{c \in R^{n+1}} \|b - Ac\|^2 = \left(A^T A \right)^{-1} A^T b \qquad (18)$$

However, A may not be even of full rank matrix, i.e., $rank(A) = r < n + 1$, in which case, $A^T A$ will be *singular* and the inverse cannot be computed. To address this problem, we make use of the Singular Value Decomposition (SVD) of A as follows,

$$A = U \Sigma V^T = \sum_{i=1}^{r} \sigma_i u_i v_i^T \qquad (19)$$

where U and V are mxm and $(n+1)x(n+1)$ orthogonal matrices which holds the eigenvectors of the square matrices, AA^T and $A^T A$, respectively, as the column vectors. The $mx(n+1)$ matrix, Σ, can be expressed as,

$$\Sigma = \begin{bmatrix} \sigma_1 & 0 & 0 & \dots & 0 & 0 & \dots & 0 \\ 0 & \sigma_2 & 0 & \dots & 0 & 0 & \dots & 0 \\ 0 & 0 & \sigma_3 & \dots & 0 & 0 & \dots & 0 \\ \dots & \dots & \dots & \dots & \dots & \dots & \dots & 0 \\ 0 & 0 & 0 & \dots & \sigma_r & 0 & \dots & 0 \\ 0 & 0 & 0 & \dots & 0 & 0 & \dots & 0 \\ \dots & \dots & \dots & \dots & \dots & \dots & \dots & \dots \\ 0 & 0 & 0 & 0 & 0 & 0 & \dots & 0 \end{bmatrix} \qquad (20)$$

where $\sigma_1 > \sigma_2 > \dots > \sigma_r$ are the singular values or equivalently the eigenvalues of matrices, $A^T A$ and AA^T. This can yield the LS solution, c^{LS}, regardless whether or not A is singular,

$$c^{LS} = V \Sigma^{-1} U^T b = \sum_{i=1}^{r} \frac{1}{\sigma_i} v_i u_i^T b \qquad (21)$$

However, the LS solution, c^{LS}, can still yield large values, the so-called "explosion" of the LS solution, due to noisy values in matrix A (the input = powers of x coordinates of the m points) or in vector b (the output = y coordinates of the m points), or both. A crucial disadvantage here is that the smaller non-zero singular values will result in even larger explosion of c^{LS}. In order to prevent this, we shall *regularize* the LS solution by optimizing the LS error together with the magnitude of the LS solution as,

$$c^{RLS} = \min_{c \in R^{n+1}} (\|b - Ac\|^2 + \lambda^2 \|c\|^2) \qquad (22)$$

IEEE Access·

S. Kiranyaz *et al.*: Left Ventricular Wall Motion Estimation by Active Polynomials for Acute Myocardial Infarction Detection

where λ is the regularization parameter. It is straightforward to show that this joint optimization can be expressed as,

$$c^{RLS} = \min_{c \in R^{n+1}} \left\| \begin{pmatrix} b \\ 0 \end{pmatrix} - \begin{pmatrix} A \\ \lambda I \end{pmatrix} c \right\|^2 = \min_{c \in R^{n+1}} \|b_\lambda - A_\lambda c\|^2 \tag{23}$$

where A_λ is now an $(m + n + 1) \times (n + 1)$ full-rank matrix $(r=n+1)$ and therefore, the LS solution over A_λ can be obtained by using Eq. (18) as,

$$c^{LS}(\lambda) = \min_{c \in R^{n+1}} \|b_\lambda - A_\lambda c\|^2 = \left(A_\lambda^T A_\lambda\right)^{-1} A_\lambda^T b_\lambda$$

$$= \left(A^T A + \lambda^2 I\right)^{-1} A^T b \tag{24}$$

The ith eigenvector of $\left(A_\lambda^T A_\lambda\right)$ can be obtained by solving,

$$A_\lambda^T A_\lambda v_i = \left(A^T A + \lambda^2 I\right) v_i = \left(\sigma_i^2 + \lambda^2\right) v_i \tag{25}$$

So it is clear that matrix $A_\lambda^T A_\lambda$ has the same eigenvector, v_i, as matrix $A^T A$ but a larger eigenvalue, $\left(\sigma_i^2 + \lambda^2\right)$. Therefore, using the orthogonality of the eigenvectors, one can write the eigenvector decomposition of $A_\lambda^T A_\lambda$, and its inverse as follows:

$$A_\lambda^T A_\lambda = \sum_{j=1}^{n+1} \left(\sigma_j^2 + \lambda^2\right) v_j v_j^T = V \Lambda V^T$$

$$\left(A_\lambda^T A_\lambda\right)^{-1} = = \sum_{j=1}^{n+1} \frac{1}{\left(\sigma_j^2 + \lambda^2\right)} v_j v_j^T = V \Lambda^{-1} V^T \tag{26}$$

Finally, using Eqs. (19) and (26) yields the regularized LS solution, c^{RLS}, expressed as,

$$c^{RLS} = c^{LS}(\lambda) = \left(A_\lambda^T A_\lambda\right)^{-1} A^T b$$

$$= \left(\sum_{j=1}^{n+1} \frac{1}{\sigma_j^2 + \lambda^2} v_j v_j^T\right) \left(\sum_{i=1}^{r} \sigma_i v_i u_i^T\right) b$$

$$= \left(\sum_{j=1}^{r} \frac{\sigma_j}{\sigma_j^2 + \lambda^2} v_j u_j^T b\right) \tag{27}$$

A direct comparison of Eq. (21) and (27) will reveal the fact that the regularized LS solution will no longer be effected from the noisy eigenvectors with very small eigenvalues, σ_j since the when $\sigma_j \to 0$, also $\frac{\sigma_j}{\sigma_j^2 + \lambda^2} \to 0$ too with a reasonable choice of the regularization parameter, λ (e.g., $\lambda \geq 0.1$).

C. COMPUTATIONAL COMPLEXITY ANALYSIS

In this appendix, we shall first detail the computational complexities of the three main blocks: Active Contours (snakes) with N vertices, n^{th} order polynomial fitting and motion (displacement) computation of each segment.

1) ACTIVE CONTOURS

The active contour method used in the proposed method is Chan-Vese [34] which defines a minimization problem of an energy-based segmentation. The energy functional $F(c_1, c_2, C)$ is defined by [34] is as follows;

$$F(c_1, c_2, C) = \mu.Length(C) + v.Area(inside(C))$$

$$+ \lambda_1 \int_{inside(C)} |u_0(x, y) - c_1|^2 \, dxdy$$

$$+ \lambda_2 \int_{outside(C)} |u_0(x, y) - c_2|^2 \, dxdy \tag{28}$$

where $\mu \geq 0$, $v \geq 0$ and $\lambda_1, \lambda_2 > 0$ are the fixed parameters. The algorithm has a complexity of $O(mn)$ for each iteration $(N = 300)$ where m is the number of rows and, n is the number of columns in the image. The sizes of the echo records in the dataset vary from 422×636 to 768×1024 pixels.

2) n^{th} ORDER POLYNOMIAL FITTING

The regularized LS solution for the nth order polynomial fitting to the m points in 2D is expressed in Eq. (15). The regularized LS solution, c^{RLS} is expressed as,

$$c^{RLS} = c^{LS}(\lambda) = \left(A_\lambda^T A_\lambda\right)^{-1} A^T b \tag{29}$$

which can be expressed as a linear system as follows:

$$\left(A_\lambda^T A_\lambda\right) c^{RLS} = A^T b \tag{30}$$

where A_λ is an $(m + n + 1) \times (n + 1)$ full-rank matrix and hence $\left(A_\lambda^T A_\lambda\right)$ is a $(n + 1) \times (n + 1)$ is a full-rank square matrix, $A^T b$ is a $n \times 1$ column vector. The solution of a linear system, $Ax=b$ where A is an $n \times n$ full-rank matrix is in $O(n^3)$ in the worst case. This is negligible in this application since 4th order polynomials are used both for RPs and APs, and thus $n + 1 = 5$ is the rank of the matrix A. Since we have m points in 2D surface, $p_i = (x_i, y_i)$, $i = 1..m$, and $m \gg n$, the significant computational complexity will result from the matrix multiplication, $A_\lambda^T A_\lambda$, which is in $O(n^2(m + n))$ and matrix-vector multiplication,, which is in $O(nm)$. Therefore, both computational complexities are linearly proportional with the number of 2D points, m.

3) SEGMENT MOTION ESTIMATION AND LVEF COMPUTATION

This is the least computationally demanding block of all since the segment displacement can be approximated by averaging the point-wise distances as expressed in Eq.(3). With L_2 norm and $n_s = 5$ points, this requires only 5 summations and 10 differences, a total of 15 summation operation, which is negligible. This will be repeated by 6 segments for each frame in the echo, and for all frames so as to compute the maximum displacement of each segment. Similarly, the LVEF computation is even simpler than the segment-wise motion estimation since it requires only the counting (incrementing) the number of pixels inside the evolved snake.

S. Kiranyaz *et al.*: Left Ventricular Wall Motion Estimation by Active Polynomials for Acute Myocardial Infarction Detection

IEEE *Access*

TABLE 7. Execution time percentages of each block of the proposed method illustrated in Figure 5.

Process	*Time (%)*
RPs	17.45
Snake	78.15
APs	0.25
LVEF	0.19
Disp. Ratio	0.057

4) COMPUTATIONAL TIMES

In the current un-parallelized and un-optimized MATLAB (version 2018a) implementation of the proposed method over a PC with 3.2GHz CPU and 16GB memory, the total execution time to process a cardiac cycle is about 36.9 seconds by 2 seconds per frame. The individual time share of each operation as illustrated in Figure 5 is given in Table 7. It is obvious that the majority of the computational complexity arises from the formation of the snake and then the formation of the both types of polynomials, RPs and APs.

ACKNOWLEDGMENT

REFERENCES

[1] K. Thygesen, J. S. Alpert, and H. D. White, "Universal definition of myocardial infarction," *Circulation*, vol. 116, no. 22, pp. 2634–2653, 2007.

[2] K. Thygesen, J. S. Alpert, A. S. Jaffe, M. L. Simoons, B. R. Chaitman, and H. D. White, "Third universal definition of myocardial infarction," *Rev. Esp. Cardiol.*, vol. 66, p. 232, Apr. 2013, doi: 10.1016/j.rec.2012.11.006.

[3] V. Sudarshan, U. R. Acharya, E. Y.-K. Ng, C. S. Meng, R. S. Tan, and D. N. Ghista, "Automated identification of infarcted myocardium tissue characterization using ultrasound images: A review," *IEEE Rev. Biomed. Eng.*, vol. 8, pp. 86–97, 2015.

[4] J. Konrad and E. Dubois, "Bayesian estimation of motion vector fields," *IEEE Trans. Pattern Anal. Mach. Intell.*, vol. 14, no. 9, pp. 910–927, Sep. 1992.

[5] R. C. Kordasiewicz, M. D. Gallant, and S. Shirani, "Affine motion prediction based on translational motion vectors," *IEEE Trans. Circuits Syst. Video Technol.*, vol. 17, no. 10, pp. 1388–1394, Oct. 2007.

[6] M. Dandel, H. Lehmkuhl, C. Knosalla, N. Suramelashvili, and R. Hetzer, "Strain and strain rate imaging by Echocardiography–Basic concepts and clinical applicability," *Current Cardiol. Rev.*, vol. 5, no. 2, pp. 133–148, May 2009.

[7] H. A. Omar, A. Patra, J. S. Domingos, P. Leeson, and A. J. Noblel, "Automated myocardial wall motion classification using handcrafted features vs a deep CNN-based mapping," in *Proc. 40th Annu. Int. Conf. IEEE Eng. Med. Biol. Soc. (EMBC)*, Jul. 2018, pp. 3140–3143. [Online]. Available: https://doi.org/10.1109/EMBC.2018.8513063

[8] A. Heimdal, A. Støylen, H. Torp, and T. Skjærpe, "Real-time strain rate imaging of the left ventricle by ultrasound," *J. Amer. Soc. Echocardiography*, vol. 11, no. 11, pp. 1013–1019, Nov. 1998.

[9] M. Bansal and P. P. Sengupta, "Speckle tracking echocardiography," in *Perioperative Transesophageal Echocardiography*. Amsterdam, The Netherlands: Elsevier, 2014, pp. 298–300.

[10] M. Tee, J. A. Noble, and D. A. Bluemke, "Imaging techniques for cardiac strain and deformation: Comparison of echocardiography, cardiac magnetic resonance and cardiac computed tomography," *Expert Rev. Cardiovascular Therapy*, vol. 11, no. 2, pp. 221–231, Feb. 2013.

[11] O. A. Smiseth, H. Torp, A. Opdahl, K. H. Haugaa, and S. Urheim, "Myocardial strain imaging: How useful is it in clinical decision making?" *Eur. Heart J.*, vol. 37, no. 15, pp. 1196–1207, Apr. 2016.

[12] A. S. A. S. Solomon, "Myocardial deformation imaging: Current status and future directions," *Circulation*, vol. 125, no. 2, pp. e244–e248, 2012.

[13] J. H. Riffel, M. G. P. Keller, M. Aurich, Y. Sander, F. Andre, S. Giusca, F. aus dem Siepen, S. Seitz, C. Galuschky, G. Korosoglou, D. Mereles, H. A. Katus, and S. J. Buss, "Assessment of global longitudinal strain using standardized myocardial deformation imaging: A modality independent software approach," *Clin. Res. Cardiol.*, vol. 104, no. 7, pp. 591–602, Jul. 2015.

[14] A. Stoylen, "Basic strain ultrasound for clinicians. Principles and technology for strain and strain rate imaging by echocardiography," Norwegian Univ. Sci. Technol., Trondheim, Norway, Tech. Rep., Jun. 2016. [Online]. Available: http://folk.ntnu.no/stoylen/strainrate/measurements.html

[15] Y. Nagata, M. Takeuchi, K. Mizukoshi, V. C.-C. Wu, F.-C. Lin, K. Negishi, S. Nakatani, and Y. Otsuji, "Intervendor variability of two-dimensional strain using vendor-specific and vendor-independent software," *J. Amer. Soc. Echocardiography*, vol. 28, no. 6, pp. 630–641, Jun. 2015.

[16] J.-U. Voigt, G. Pedrizzetti, P. Lysyansky, T. H. Marwick, H. Houle, R. Baumann, S. Pedri, Y. Ito, Y. Abe, S. Metz, J. H. Song, J. Hamilton, P. P. Sengupta, T. J. Kolias, J. d'Hooge, G. P. Aurigemma, J. D. Thomas, and L. P. Badano, "Definitions for a common standard for 2D speckle tracking echocardiography: Consensus document of the EACVI/ASE/Industry task force to standardize deformation imaging," *J. Amer. Soc. Echocardiography*, vol. 28, no. 2, pp. 183–193, Feb. 2015.

[17] P. Biaggi, S. Carasso, P. Garceau, M. Greutmann, C. Gruner, W. Tsang, H. Rakowski, Y. Agmon, and A. Woo, "Comparison of two different speckle tracking software systems: Does the method matter?" *Echocardiography*, vol. 28, no. 5, pp. 539–547, May 2011.

[18] S. A. Coulter, "Echocardiographic evaluation of coronary artery disease," in *Coronary Artery Disease*. London, U.K.: Springer, 2015, pp. 217–252.

[19] M. Leitman, P. Lysyansky, S. Sidenko, "Two-dimensional strain–a novel software for real-time quantitative echocardiographic assessment of myocardial function," *J. Amer. Soc. Echocardiography*, vol. 17, no. 10, pp. 1021–1029, 2004, doi: 10.1016/j.echo.2004.06.019.

[20] F. Jamal, J. Strotmann, F. Weidemann, T. Kukulski, J. D'Hooge, B. Bijnens, F. Van de Werf, I. De Scheerder, and G. R. Sutherland, "Noninvasive quantification of the contractile reserve of stunned myocardium by ultrasonic strain rate and strain," *Circulation*, vol. 104, no. 9, pp. 1059–1065, 2001.

[21] M. Bansal, L. Jeffriess, R. Leano, J. Mundy, and T. H. Marwick, "Assessment of myocardial viability at dobutamine echocardiography by deformation analysis using tissue velocity and speckle-tracking," *JACC: Cardiovascular Imag.*, vol. 3, no. 2, pp. 121–131, 2010.

[22] M. Becker, R. Hoffmann, H. P. Kuhl, M. Grawe, M. Katoh, R. Kramann, A. Bucker, P. Hanrath, and N. Heussen, "Analysis of myocardial deformation based on ultrasonic pixel tracking to determine transmurality in chronic myocardial infarction," *Eur. Heart J.*, vol. 27, no. 21, pp. 2560–2566, Sep. 2006.

[23] V. Delgado, R. J. van Bommel, M. Bertini, C. J. W. Borleffs, N. A. Marsan, A. C. T. Ng, G. Nucifora, N. R. L. van de Veire, C. Ypenburg, E. Boersma, E. R. Holman, M. J. Schalij, and J. J. Bax, "Relative merits of left ventricular dyssynchrony, left ventricular lead position, and myocardial scar to predict long-term survival of ischemic heart failure patients undergoing cardiac resynchronization therapy," *Circulation*, vol. 123, no. 1, pp. 70–78, Jan. 2011.

[24] M. Kass, A. Witkin, and D. Terzopoulos, "Snake: Active contour model," *Int.J. Comput. Vis.*, vol. 1, pp. 321–331, Apr. 1987.

[25] L. Juan and O. Gwun, "A comparison of SIFT, PCA-SIFT and SURF," *Int. J. Image Process.*, vol. 3, no. 4, pp. 143–152, 2009.

[26] D. Mistry and A. Banerjee, "Comparison of feature detection and matching approaches: SIFT and SURF," *GRD J.-Global Res. Develop. J. Eng.*, vol. 2, no. 4, pp. 7–13, Mar. 2017.

[27] T. Tuytelaars, K. Mikolajczyk, "Local invariant feature detectors: A survey," in *Foundations and Trends in Computer Graphics and Vision*, vol. 3, no. 3. Norwell, MA, USA: Now Publishers Inc., 2007, pp. 177–280, doi: 10.1561/0600000017.

[28] A. Canclini, M. Cesana, A. Redondi, M. Tagliasacchi, J. Ascenso, and R. Cilla, "Evaluation of low-complexity visual feature detectors and descriptors," in *Proc. 18th Int. Conf. Digit. Signal Process. (DSP)*, Jul. 2013, pp. 1–7, doi: 10.1109/ICDSP.2013.6622757.

[29] M. Qazi, G. Fung, S. Krishnan, R. Rosales, H. Steck, B. Rao, D. D. Poldermans, and D. Chandrasekaran, "Automated heart wall motion abnormality detection from ultrasound images using Bayesian networks," in *Proc. Int. Joint Conf. Artif. Intell.*, 2007, pp. 1–7.

IEEE Access

S. Kiranyaz *et al.*: Left Ventricular Wall Motion Estimation by Active Polynomials for Acute Myocardial Infarction Detection

[30] G. Carneiro and J. C. Nascimento, "Combining multiple dynamic models and deep learning architectures for tracking the left ventricle endocardium in ultrasound data," *IEEE Trans. Pattern Anal. Mach. Intell.*, vol. 35, no. 11, pp. 2592–2607, Nov. 2013.

[31] S. Dong, G. Luo, G. Sun, K. Wang, and H. Zhang, "A left ventricular segmentation method on 3D echocardiography using deep learning and snake," in *Proc. Comput. Cardiol. Conf. (CinC)*, Sep. 2016, pp. 473–476.

[32] G. Luo, R. An, K. Wang, S. Dong, and H. Zhang, "A deep learning network for right ventricle segmentation in short-axis MRI," in *Proc. Comput. Cardiol. Conf. (CinC)*, Sep. 2016, pp. 485–488.

[33] G. Carneiro, J. C. Nascimento, and A. Freitas, "The segmentation of the left ventricle of the heart from ultrasound data using deep learning architectures and derivative-based search methods," *IEEE Trans. Image Process.*, vol. 21, no. 3, pp. 968–982, Mar. 2012.

[34] A. Shalbaf, H. Behnam, Z. Alizade-Sani, and M. Shojaifard, "Left ventricle wall motion quantification from echocardiographic images by non-rigid image registration," *Int. J. Comput. Assist. Radiol. Surg.*, vol. 7, no. 5, pp. 769–783, Sep. 2012, doi: 10.1007/s11548-012-0786-2.

[35] B. D. Lucas and T. Kanade, "An iterative image registration technique with an application to stereo vision," in *Proc. 7th Int. Jt. Conf. Artif. Intell.*, Apr. 1981, pp. 121–130.

[36] M. N. O. Landgren Christian and A. Heyden, "Segmentation of the left heart ventricle in ultrasound images using a region based snake," *Proc. SPIE*, vol. 8669, Mar. 2013, Art. no. 866945.

[37] J. Pedrosa, S. Queiros, O. Bernard, J. Engvall, T. Edvardsen, E. Nagel, and J. D'hooge, "Fast and fully automatic left ventricular segmentation and tracking in echocardiography using shape-based B-Spline explicit active surfaces," *IEEE Trans. Med. Imag.*, vol. 36, no. 11, pp. 2287–2296, Nov. 2017, doi: 10.1109/TMI.2017.2734959.

[38] D. Barbosa, T. Dietenbeck, J. Schaerer, J. D'hooge, D. Friboulet, and O. Bernard, "B-spline explicit active surfaces: An efficient framework for real-time 3-D region-based segmentation," *IEEE Trans. Image Process.*, vol. 21, no. 1, pp. 241–251, Jan. 2012, doi: 10.1109/TIP.2011.2161484.

[39] M. Marsousi, A. Eftekhari, A. Kocharian, and J. Alirezaie, "Endocardial boundary extraction in left ventricular echocardiographic images using fast and adaptive B-spline snake algorithm," *Int. J. Comput. Assist. Radiol. Surgery*, vol. 5, no. 5, pp. 501–513, Sep. 2010, doi: 10.1007/s11548-010-0404-0.

[40] R. M. Lang, "Recommendations for chamber quantification: A report from the American Society of echocardiography's guidelines and standards committee and the chamber quantification writing group, developed in conjunction with the European Association of echocardiography, a branch of the European society of cardiology," *J. Amer. Soc. Echocardiography*, vol. 18, no. 12, pp. 1440–1463, 2005.

[41] T. F. Chan and L. A. Vese, "Active contours without edges," *IEEE Trans. Image Process.*, vol. 10, no. 2, pp. 266–277, Feb. 2001.

AYSEN DEGERLI received the B.Sc. degree (Hons.) in electrical and electronics engineering from the Izmir University of Economics, Turkey, in 2017, and the M.Sc. degree (Hons.) in data engineering and machine learning from Tampere University, Finland, in 2019. She is currently pursuing the Ph.D. degree in computing and electrical engineering with the Signal Analysis and Machine Intelligence research group led by Prof. M. Gabbouj with Tampere University. Her research interests include machine learning, compressive sensing, and biomedical image processing.
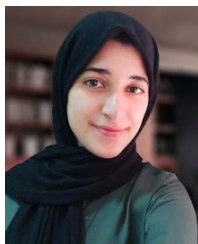
TAHIR HAMID has been working as an Interventional Cardiology Consultant with the Heart Hospital, Hamad Medical Corporation, Doha, Qatar. He has been trained in U.K. and with the University of Toronto, Canada. He has about 27 publications and presented at various cardiology conferences. Currently, conducting randomized control trial about "pre-procedural fasting in patients undergoing coronary interventions" at the Toronto General Hospital, University of Toronto. He has published the following study related to ECG monitoring in patients with recurrent blackouts: "Prolonged implantable electrocardiographic monitoring indicates a high rate of misdiagnosis of epilepsy - REVISE study", Europace. This study revolutionized the assessment of patient blackout that were wrongly labeled as epileptics and were later found after prolonged monitoring, to have cardiac rhythm related issues leading to blackouts. He is also actively involved in the research projects at Hamad Medical Corporation. He is also working on his project about external cardiopulmonary resuscitation devices for patients who sustain cardiac arrests.

RASHID MAZHAR has more than 20 years of experience in the field of cardiothoracic surgery. He is currently a Senior Consultant Thoracic surgeon with Hamad General Hospital, Doha, Qatar, with minimal invasive & Robotic surgery as his areas of surgical interest. Besides his surgical, clinical and educational activities, he has a particular interest and track record of translational research, collaborating with engineers and academicians to bring about user-end driven innovative medical solutions. Automation, objective monitoring, intensive care, cardio-pulmonary resuscitation, and user-friendly signal processing are his areas of interest. His research projects at HMC and Qatar foundation has obtained grant funds in excess of 5 Million Qatari riyals. These include five HMC, two UREP and three NPRP funded projects. He is currently part of two ongoing NPRP funded projects. To his credit, he has more than 30 publications, including a book chapter; four granted patents, four patents under process, five HMC innovations award, and four Stars of excellence awards in research category.

SERKAN KIRANYAZ (Senior Member, IEEE) is currently a Professor with Qatar University, Doha, Qatar. He has published two books, five book chapters, more than 70 journal articles in high impact journals, and 100 papers in international conferences. He made contributions on evolutionary optimization, machine learning, bio-signal analysis, computer vision with applications to recognition, classification, and signal processing. He has coauthored the articles which have nominated or received the "Best Paper Award" in ICIP 2013, ICPR 2014, ICIP 2015, and IEEE TSP 2018. He had the most-popular articles in the years 2010 and 2016, and most-cited article in 2018 in IEEE Transactions on Biomedical Engineering. From 2010 to 2015, he has authored the most-cited article of the *Neural Networks* journal. His research team has won the 2nd and 1st places in PhysioNet Grand Challenges 2016 and 2017, among 48 and 75 international teams, respectively. In 2019, he won the "Research Excellence Award" and "Merit Award" of Qatar University. His theoretical contributions to advance the current state of the art in modeling and representation, targeting high long-term impact, while algorithmic, system level design and implementation issues target medium and long-term challenges for the next five to ten years. He in particular aims at investigating scientific questions and inventing cutting edge solutions in "personalized biomedicine" which is in one of the most dynamic areas where science combines with technology to produce efficient signal and information processing systems meeting the high expectation of the users.

RAYYAN EL FADIL AHMED received the B.Sc. degree in electrical engineering from Qatar University, in 2018. She is currently pursuing the M.Sc. degree in data science and engineering with Hamad Bin Khalifa University, Qatar. She has published work in Elsevier *Sensors and Actuators Journal*. Her research interests include computer vision, machine learning, and pattern recognition.

S. Kiranyaz *et al.*: Left Ventricular Wall Motion Estimation by Active Polynomials for Acute Myocardial Infarction Detection

IEEE *Access*

RAYAAN ABOUHASERA received the bachelor's degree in electrical engineering with a minor in computer science from Qatar University, Qatar, in 2019. She is currently pursuing the master's degree in data science and engineering with Hamad Bin Khalifa University, Qatar. Additionally, she is also working on mobile application developing. She had two published articles in the field of sensors. Her current research interests include computer vision and machine learning in medical field.

MORTEZA ZABIHI (Member, IEEE) was born in Iran, in 1988. He received the M.Sc. degree in biomedical engineering from Tampere University, Tampere, Finland, in 2013, and the Ph.D. degree from the Department of Computing Sciences, Tampere University. He is also working as a Researcher with the Department of Computing Sciences. His research interests include nonlinear dynamics and time series analysis, pattern recognition, and machine learning with application to EEG and ECG signal processing. Since 2015, he has been ranked in the top three teams in four international competitions, such as PhysioNet/Computing in Cardiology and IEEE EMBS Neural Engineering Brain-Computer Interface Challenges.

JUNAID MALIK received the bachelor's degree in electrical engineering from the National University of Science and Technology, Pakistan, in 2013, and the M.Sc. degree in information technology with a major in signal processing from the Tampere University of Technology, in 2017. He is currently pursuing the Ph.D. degree from Tampere University, Finland. He is also working with the SAMI research group as a Doctoral Researcher. His research interests include salient object segmentation, discriminative learning-based image restoration, and operational neural networks.

RIDHA HAMILA (Senior Member, IEEE) received the M.Sc., Lic.Tech. (Hons.), and Ph.D. degrees from the Tampere University of Technology (TUT), Tampere, Finland, in 1996, 1999, and 2002, respectively. From 1994 to 2002, he held various research and teaching positions at the Department of Information Technology, TUT. From 2002 to 2003, he was a System Specialist with the Nokia research Center and Nokia Networks, Helsinki. From 2004 to 2009, he was with Emirates Telecommunications Corporation, UAE. Also, from 2004 to 2013, he was an Adjunct Professor with the Department of Communications Engineering, TUT. He is currently a Full Professor with the Department of Electrical Engineering, Qatar University, Qatar. His current research interests include mobile and broadband wireless communication systems, mobile edge computing, internet of everything, and machine learning. In these areas, he has published over 200 journal and conference papers most of them in the peered reviewed IEEE publications, filed seven U.S. patents, and wrote numerous confidential industrial research reports. He has been involved in several past and current industrial projects, Ooreedo, Qatar National Research Fund, Finnish Academy projects, and EU research and education programs. He has supervised a large number of under/graduate students and Postdoctoral Fellows. He organized many international workshops and conferences.

MONCEF GABBOUJ (Fellow, IEEE) is currently a well-established world expert in the field of image processing, and held the prestigious post of Academy of Finland Professor from 2011 to 2015. He has been leading the Multimedia Research Group for nearly 25 years and managed successfully a large number of projects in excess of 18M Euro. He has supervised 45 Ph.D. theses and over 50 M.Sc. theses. He is the author of several books and over 700 articles. His research interests include big data analytics, multimedia content-based analysis, indexing and retrieval, artificial intelligence, machine learning, pattern recognition, nonlinear signal and image processing and analysis, voice conversion, and video processing and coding. He is also a member of the Academia Europaea and the Finnish Academy of Science and Letters. He is also the past Chairman of the IEEE CAS TC on DSP and a Committee member of the IEEE Fourier Award for Signal Processing. He has served as an Associate Editor and a Guest Editor for many IEEE, and international journals.

• • •